Supporting Information

Rapid SARS-CoV-2 Spike Protein Detection by Carbon Nanotube-Based Near-Infrared Nanosensors

Rebecca L. Pinals,[1] Francis Ledesma,[1] Darwin Yang,[1] Nicole Navarro,[2] Sanghwa Jeong,[1] John E. Pak,[3] Lili Kuo,[4] Yung-Chun Chuang,[5,6], Yu-Wei Cheng,[5] Hung-Yu Sun,[7] Markita P. Landry[1,3,8,9]*

[1] Department of Chemical and Biomolecular Engineering, University of California, Berkeley, California 94720, United States

[2] Department of Chemistry, University of California, Berkeley, California 94720, United States

[3] Chan-Zuckerberg Biohub, San Francisco, California 94158, United States

[4] Wadsworth Center, New York State Department of Health, Slingerlands, New York 12159, United States

[5] Leadgene Biomedical Inc., Tainan 71042, Taiwan

[6] Department of Medical Laboratory Science and Biotechnology, College of Medicine, National Cheng Kung University, Tainan 70101, Taiwan

[7] Institute of Molecular Medicine, College of Medicine, National Cheng Kung University, Tainan 70101, Taiwan

[8] Innovative Genomics Institute (IGI), Berkeley, California 94720, United States

[9] California Institute for Quantitative Biosciences, QB3, University of California, Berkeley, California 94720, United States

Methods

Synthesis of ssDNA-SWCNTs

Suspensions of single-walled carbon nanotube (SWCNTs) with single-stranded DNA (ssDNA) were prepared by mixing 0.2 mg of mixed-chirality SWCNTs (small diameter HiPco™ SWCNTs, NanoIntegris) with 250 μM of ssDNA (custom ssDNA oligos with standard desalting, Integrated DNA Technologies, Inc.) in 1 mL, 0.1X phosphate-buffered saline (PBS; note 1X is 137 mM NaCl, 2.7 mM KCl, 10 mM Na_2HPO_4, 1.8 mM KH_2PO_4). This mixture was bath sonicated for 30 min (Branson Ultrasonic 1800) then probe-tip sonicated for 10 min in an ice bath (3 mm probe tip at 50% amplitude, 5-6 W, Cole-Parmer Ultrasonic Processor). Suspensions were centrifuged to pellet insoluble SWCNT bundles and contaminants (16.1 krcf, 90 min). Supernatant was collected and ssDNA-SWCNT concentration was calculated with measured sample absorbance at 632 nm (NanoDrop One, Thermo Scientific) and the empirical extinction coefficient ε_{632nm}=0.036 L mg^{-1} cm^{-1}.[1] ssDNA-SWCNTs were stored at 4°C and diluted to a working concentration of 10 mg L^{-1} in 1X PBS at ambient temperature ≥ 2 h prior to use.

Preparation of proteins and biofluids

Proteins were sourced and reconstituted as listed in **Table S1**. All viral protein analytes were purified with desalting columns to remove impurities (Zeba Spin Desalting Columns, 0.5 mL with 7 kDa MWCO, Thermo Fisher Scientific) by washing with PBS three times (1500 rcf for 1 min), centrifuging with sample (1500 rcf for 2 min), and retaining sample in flow-through solution. Resulting protein concentration was measured with the Qubit Protein Assay (Thermo Fisher Scientific) and proteins were diluted in PBS to 10X the intended final analyte concentration.

Biofluids were prepared by centrifuging to remove any large contaminants (1000 rcf for 5 min) then diluting in PBS to 10X the intended final concentration. Sputasol (Oxoid) was used to liquify sputum prior to use, used according to manufacturer's instructions.

Synthesis of ACE2-ssDNA-SWCNT nanosensors

Nanosensors were made by preparing solutions of 10 mg/L $(GT)_6$-SWCNTs and 25 mg/L ACE2, mixing in equal volumes, incubating for 30 min, diluting by half with PBS, and incubating for an additional 30 min. Final concentrations of components are thus 2.5 mg/L $(GT)_6$-SWCNTs and 6.25 mg/L ACE2. Removal of unbound ACE2 remaining in solution was attempted by centrifugal filtration (Amicon Ultra-0.5 mL centrifugal filters with 100 kDa MWCO, Millipore Sigma), however, this led to embedding of nanosensors in the filter membrane and negligible nanosensor yield. Downstream testing confirmed necessity of the bound ACE2-SWCNT complex for SARS-CoV-2 spike protein sensing, therefore, presence of free ACE2 was not a concern. For the stability

test of nIR fluorescence as a function of time, $(GT)_6$-SWCNTs and ACE2 were injected together to these final concentrations and measured immediately.

For passivation of nanosensors with phospholipid-PEG, the protocol was slightly modified to incorporate first adsorption of the sensing protein (ACE2) then passivation of remaining exposed SWCNT surface by phospholipid-PEG (saturated 16:0 phosphatidylethanolamine-PEG 5000 Da, or PE-PEG). Passivated nanosensors were made by preparing solutions of 10 mg/L $(GT)_6$-SWCNTs and 25 mg/L ACE2, mixing in equal volumes, incubating for 15 min, adding PE-PEG to a final concentration of 2.5 mg/L, diluting by half with PBS, bath sonicating for 15 min, and incubating for an additional 30 min.

Preparation of SARS-CoV-2 S RBD analyte

Plasmid encoding for SARS-CoV-2 S RBD[2] was transiently transfected into suspension Expi293 cells at 0.5-1 L scale. Three days after transfection, cell culture supernatants were clarified and purified by Ni-NTA affinity chromatography as previously described[3] and the eluted protein was dialyzed extensively against PBS prior to storage at -80C.

Synthesis and purification of SARS-CoV-2 VLPs

To prepare the SARS-CoV-2 VLPs, two plasmids pcDNA3.1-Spike and pIRES2-MNE were synthesized based on the sequence of the Wuhan-Hu-1 strain (GenBank: MN908947.3). The spike protein was stabilized with the furin cleavage (residues 682-685) abrogated and the consecutive residue 986 and 987 substituted with prolines.[4,5] The VLPs were synthesized by co-transfecting HEK293 or HEK293T cells with plasmids using HyFect transfection reagent (Leadgene Biomedical Inc., Taiwan) or JetOptimus (Polyplus-transfection, USA). To generate VLPs without S protein, cells were transfected with pIRES2-MNE only. The harvested supernatant was first concentrated with a 100 kDa MWCO centrifugal filter (Pall Corporation) then laid over discontinuous 20%-60% sucrose or Opti-prep (BioVision Inc.) gradients followed with centrifugation at 30,000 rpm for 4 hours. Purified VLPs were resuspended in PBS pH 7.4 and frozen at -80°C for storage.

Nanosensor optical characterization and analyte screening

Fluorescence was measured with an inverted Zeiss microscope (Axio Observer.D1, 10X objective) coupled to a Princeton Instruments spectrometer (SCT 320) and liquid nitrogen-cooled Princeton Instruments InGaAs detector (PyLoN-IR). Samples were excited with a triggered 721 nm laser (OptoEngine LLC) and emission was collected in the 800 – 1400 nm wavelength range, with

samples in a polypropylene 384 well-plate format (30 μL total sample volume; Greiner Bio-One microplate).

For nIR fluorescence screens, 27 μL of nanosensor was added per well and 3 μL of 10X-concentrated viral protein analytes in PBS (or buffer alone) were injected per well using a microchannel pipette (in triplicate), with brief mixing by pipetting. The plate was sealed with an adhesive seal (Bio-Rad) and spun down for 15 sec with a benchtop well plate centrifuge. Fluorescence spectra were recorded at time points of 0 min, 5 min, 10 min, and every subsequent 10 min until the max time point.

For surfactant stability tests, the screening protocol was modified as follows: 24 μL of nanosensor, 3 μL of 2.5 w/v% sodium cholate (SC), then 3 μL of 10X-concentrated viral protein analytes in PBS (or buffer alone) were added per well. Wavelength shifts were calculated by translating fluorescence spectra in 1 nm wavelength increments such that the correlation coefficient was maximized with respect to the reference state. Data processing in this manner captures the full spectrum shifting behavior.

Absorbance was measured by UV-VIS-nIR spectrophotometer (Shimadzu UV-3600 Plus) with samples in a 50 μL volume, black-sided quartz cuvette (Thorlabs, Inc.).

For surface-immobilized nanosensor experiments, ACE2-SWCNTs were immobilized on MatTek glass-bottom microwell dishes (35 mm petri dish with 10 mm microwell) as follows: the dish was washed twice with 150 μL PBS, 100 μL of nanosensor (formed by 12.5 mg/L ACE2 with 5 mg/L $(GT)_6$-SWCNT pre-incubated for 40 min) was added and incubated for 20 min, nanosensor solution was removed, and the dish was washed twice again with 150 μL PBS. Surface-immobilized nanosensors were imaged on an epifluorescence microscope (100x oil immersion objective) with an excitation of 721 nm and a Ninox VIS-SWIR 640 camera (Raptor). For each imaging experiment, 120 μL PBS was added prior to recording and the z-plane was refocused. Images were collected with a 950 ms exposure time and 1000 ms repeat cycle over 5 min. 15 μL buffer was added at frame 60 and 15 μL analyte was added at frame 120. Images were processed in ImageJ by applying a median filter (0.5-pixel radius) and rolling ball background subtraction (300-pixel radius), then using the ROI analyzer tool (Multi Measure).

Corona exchange assay

Corona dynamic studies were done as described previously.[6] Briefly, the same ssDNA-SWCNT suspension protocol was employed, instead using fluorophore-labeled ssDNA-Cy5 (3' Cy5-labeled custom ssDNA oligos with HPLC purification, Integrated DNA Technologies, Inc.). Fluorescently labeled ssDNA was tracked and the displacement of ssDNA from the SWCNT surface (monitored as in increase in Cy5 fluorescence) was used as a proxy for protein adsorption. To assess $(GT)_6$-Cy5 desorption from SWCNTs in the presence of ACE2, 25 μL of 12.5 mg L^{-1} ACE2 was added to 25 μL of 5 mg L^{-1} $(GT)_6$-Cy5-SWCNTs. To assess $(GT)_6$-Cy5 desorption

from nanosensors in the presence of S RBD, 5 µL of 10X-concentrated S RBD was injected into 45 µL of ACE2-$(GT)_6$-Cy5-SWCNTs. Solutions were added via microchannel pipette into a 96-well PCR plate (Bio-Rad) and mixed by pipetting. The plate was sealed with an optically transparent adhesive seal (Bio-Rad) and briefly spun down on a benchtop centrifuge. Fluorescence time series readings were measured in a Bio-Rad CFX96 Real Time qPCR System by scanning the Cy5 channel every 30 s at 22.5°C.

Extended Discussion and Figures

The ratio of ACE2 to $(GT)_6$-SWCNTs was chosen based on a protein footprint estimation that 28.6 ACE2 dimers fit per SWCNT in the close-packed limit (using ACE2 dimer dimensions as determined by cryo-EM[7]). This calculation translates to a mass ratio of 2.36 ACE2:SWCNT. The actual mass ratio of 2.5 ACE2:SWCNT was chosen to be just above this theoretical close-packed limit in an attempt to minimize protein spreading that arises from a large excess of nanoparticle surface available for proteins.[8] Extending to twice this mass ratio produces more quenching in the SWCNT fluorescence (**Figure S1**), yet reduced sensing ability (**Figure S2**) and colloidal stability. Thus, the mass ratio of 2.5 ACE2:SWCNT was experimentally determined to be best suited for S RBD sensing (**Figure S2**).

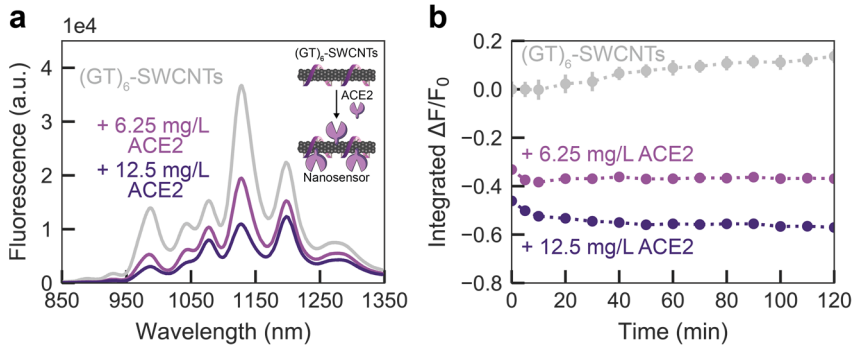

Figure S1. **Adsorption of different ratios of ACE2 on $(GT)_6$-SWCNTs.** ACE2-SWCNT complexation quenched intrinsic SWCNT near-infrared fluorescence, shown by **(a)** the full fluorescence spectrum after 1 h incubation of 6.25 mg/L or 12.5 mg/L ACE2 with 2.5 mg/L $(GT)_6$-SWCNTs (final concentrations) and **(b)** the integrated-fluorescence change as a function of time over 2 h. Both ratios exhibit stable quenched fluorescence, however, the lower ratio of protein to SWCNT exhibited better colloidal stability. Gray bars represent standard error between experimental replicates (N = 3).

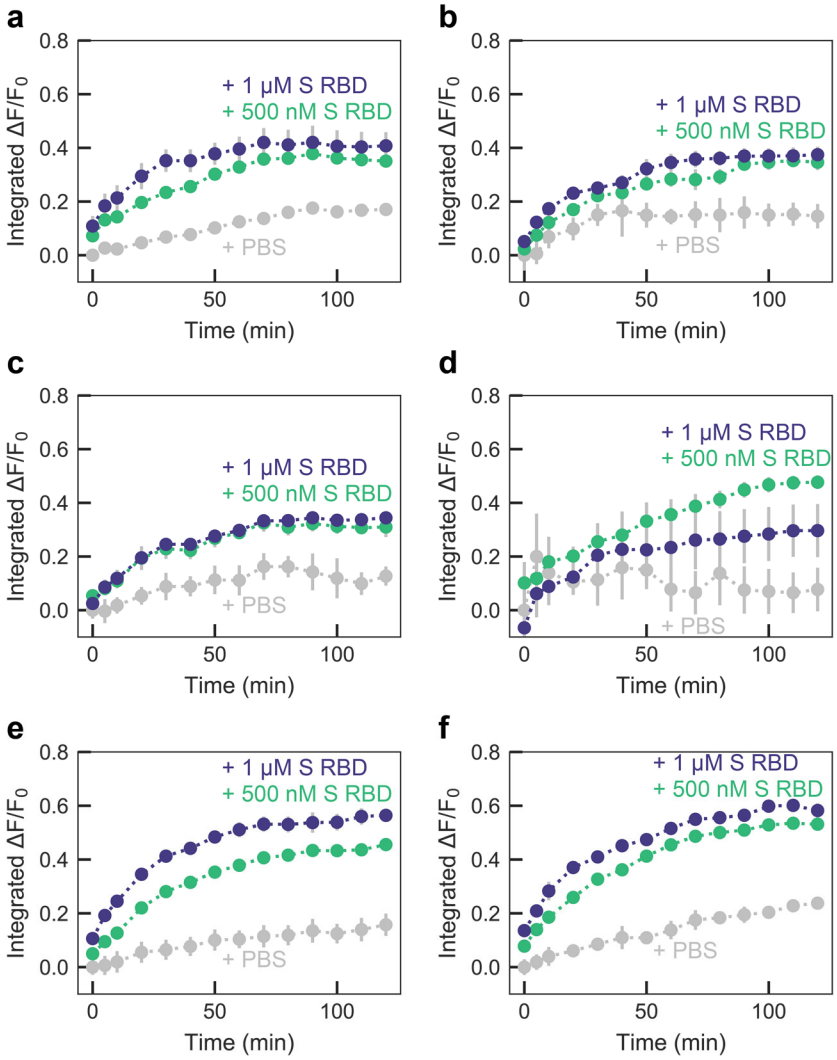

Figure S2. Response of different ratios ACE2:$(GT)_6$-SWCNTs to S RBD. Integrated-fluorescence fold change as a function of time over 120 min upon addition of PBS, 500 nM S RBD, or 1 μM S RBD to nanosensor formed by **(a)** 6.25 mg/L ACE2 and 2.5 mg/L $(GT)_6$-SWCNTs incubated 1 h, **(b)** 12.5 mg/L ACE2 and 2.5 mg/L $(GT)_6$-SWCNTs incubated 1 h, **(c)** 6.25 mg/L ACE2 and 2.5 mg/L $(GT)_6$-SWCNTs incubated 3 h, **(d)** 12.5 mg/L ACE2 and 2.5 mg/L $(GT)_6$-SWCNTs incubated 3 h, **(e)** 6.25 mg/L ACE2 and 2.5 mg/L $(GT)_6$-SWCNTs incubated 30 min, diluted by half in PBS, and incubated an additional 30 min, and **(f)** 12.5 mg/L ACE2 and 2.5 mg/L $(GT)_6$-SWCNTs incubated 30 min, diluted by half in PBS, and incubated an additional 30 min. Gray bars represent standard error between experimental replicates (N = 3).

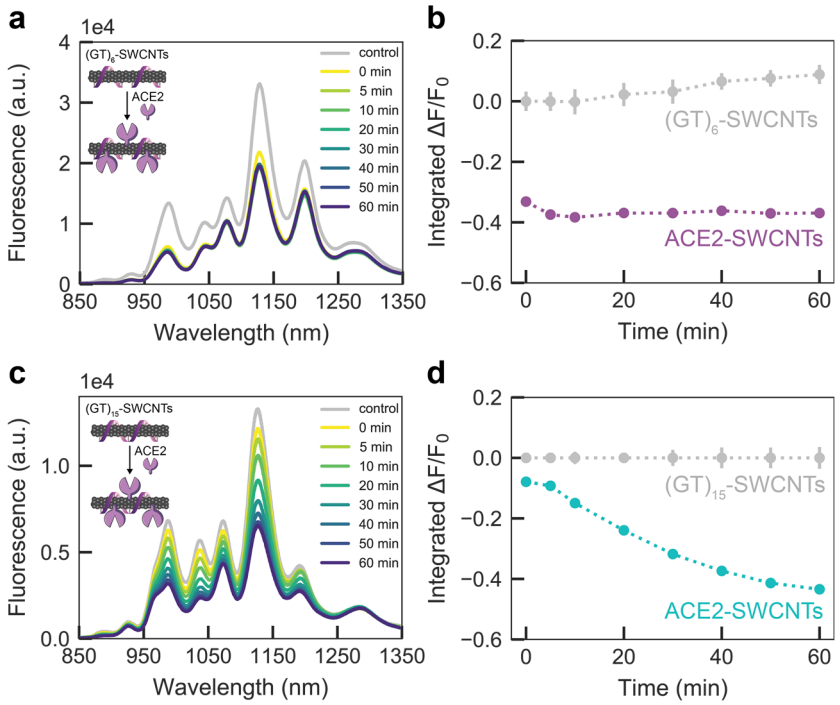

Figure S3. Adsorption of ACE2 to $(GT)_6$- vs. $(GT)_{15}$-SWCNTs. ACE2-SWCNT complexation rapidly quenched intrinsic SWCNT near-infrared fluorescence, shown by **(a)** the full fluorescence spectrum and **(b)** the integrated-fluorescence fold change as a function of time over 1 h, upon incubation of 6.25 mg/L ACE2 with 2.5 mg/L $(GT)_6$-SWCNTs (final concentrations). ACE2-SWCNT complexation quenched intrinsic SWCNT near-infrared fluorescence at a slower rate, shown by **(c)** the full fluorescence spectrum and **(d)** the integrated-fluorescence fold change as a function of time over 1 h, upon incubation of 6.25 mg/L ACE2 with 2.5 mg/L $(GT)_{15}$-SWCNTs (final concentrations). Gray bars represent standard error between experimental replicates (N = 3).

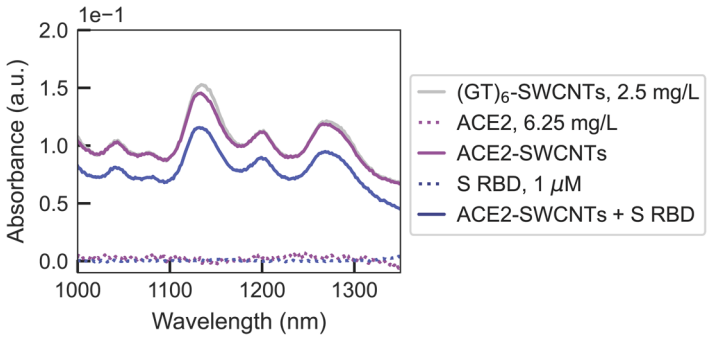

Figure S4. **Absorbance of $(GT)_6$-SWCNTs with ACE2 sensing protein and S RBD analyte.** Retention of near-infrared SWCNT absorbance peaks in the presence of ACE2 adsorption and S RBD analyte binding confirms solution-stable noncovalent passivation, rather than covalent modification, of the SWCNT surface.

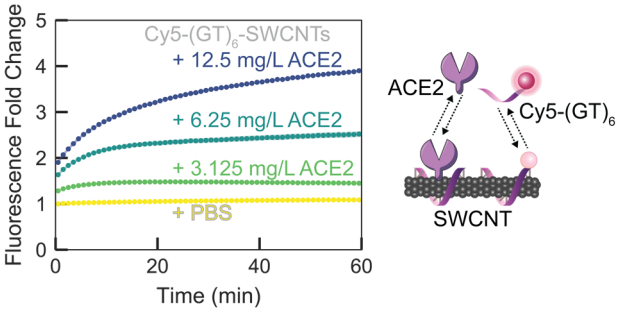

Figure S5. Displacement of Cy5-$(GT)_6$ ssDNA from SWCNT as a function of passivating ACE2 concentration. Adsorption of ACE2 on the SWCNT surface led to $(GT)_6$ desorption, tracked by Cy5-labeled ssDNA, in a concentration-dependent manner upon addition of varying ACE2 concentrations with 2.5 mg/L Cy5-$(GT)_6$-SWCNTs (final concentrations). The increase in Cy5-$(GT)_6$ fluorescence from the initial quenched state on the SWCNT serves as a proxy for ACE2 adsorption. Shaded error bars represent the standard error between experimental replicates (N = 3).

To test the stability of the ACE2-functionalized SWCNT construct, we implemented a solvatochromic shift assay.[9,10] This methodology is based upon addition of surfactant (sodium cholate, SC) that coats any solvent-exposed SWCNT surface and can displace low-affinity molecules from the SWCNT surface. SC adsorption causes exclusion of water from the SWCNT surface, producing a large increase in fluorescence and solvatochromic shift to lower emission wavelengths. Prior to ACE2 incubation, SC elicited both a large blue-shift (-16 nm) and sizeable increase in fluorescence (70.2%) for $(GT)_6$-SWCNTs alone (**Figure S6a-b**). However, upon passivation with ACE2, these spectral changes were reduced to -10 nm and 10.3%, respectively (**Figure S6c-d**), suggesting a mechanism in which ACE2 adsorbs to the SWCNT surface and

causes $(GT)_6$ ssDNA desorption. Moreover, we show that addition of S RBD analyte to the ACE2-SWCNT complex further stabilizes the nanosensor, whereby addition of SC produced a brief blue-shift of -6 nm yet a complete return to baseline by 70 min, and similarly, a minimal change in fluorescence of -3.9% (**Figure S6e-f**).

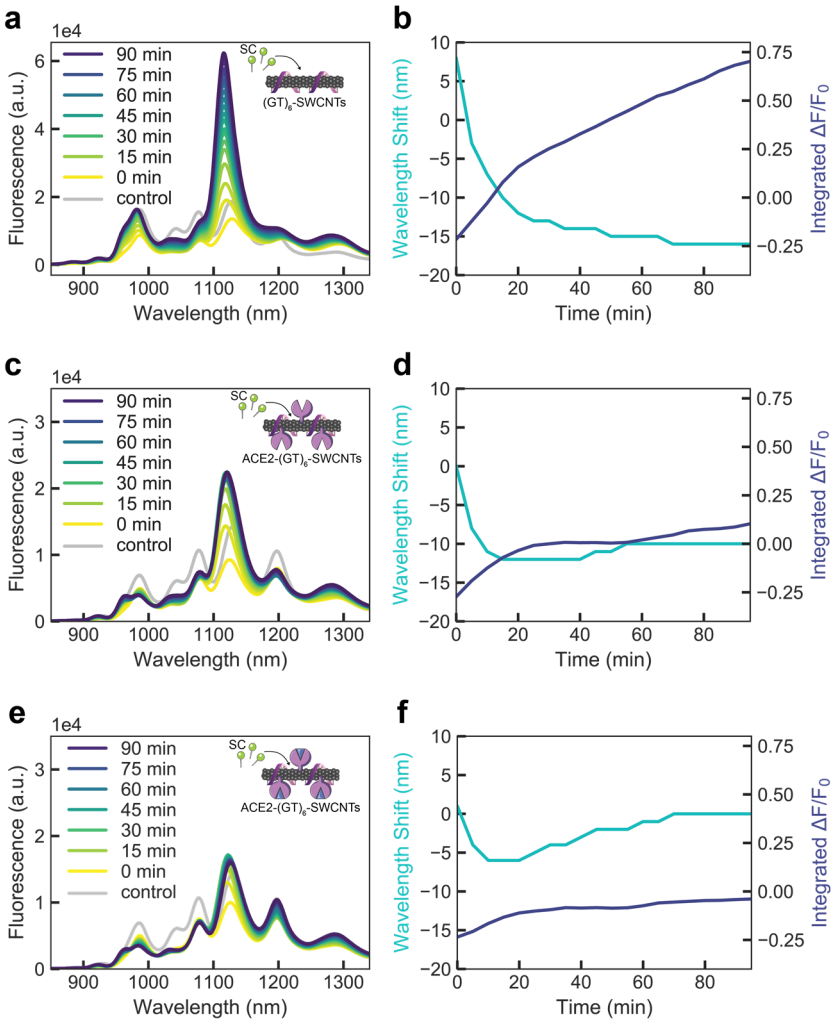

Figure S6. Surfactant displacement experiment to probe the stability of $(GT)_6$-SWCNTs with ACE2 sensing protein and S RBD analyte. Full fluorescence spectrum (left) and time-dependent wavelength shift and integrated-fluorescence fold change (right) for **(a-b)** 2.5 mg/L $(GT)_6$-SWCNTs alone, **(c-d)** ACE2-SWCNT nanosensors (formed by 6.25 mg/L ACE2 and 2.5 mg/L $(GT)_6$-SWCNTs), and **(e-f)** ACE2-SWCNT nanosensors with 500 nM S RBD, each upon addition of 0.25 w/v% sodium cholate (SC, final concentration). Decreasing blue-shift and fluorescence fold change due to ACE2 implies ACE2 covers and stabilizes the SWCNT surface, with further stabilization upon addition of S RBD analyte.

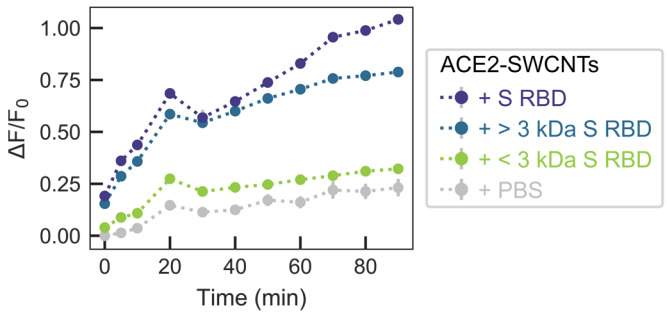

Figure S7. ACE2-SWCNT nanosensor response to controls. Addition of 500 nM S RBD (final concentration) to ACE2-SWCNTs (formed by 6.25 mg/L ACE2 and 2.5 mg/L $(GT)_6$-SWCNTs) yielded a significant turn-on fluorescence response. This response is maintained for S RBD > 3 kDa MWCO centrifugal filter and absent for S RBD < 3 kDa. Gray bars represent standard error between experimental replicates (N = 3).

The limit of detection (*LOD*) of the ACE2-SWNT nanosensor for S RBD analyte is defined as the lowest analyte concentration that can be determined to be statistically different from the blank:[11]

$$LOD = mean_{blank} + 3\,SD_{blank}$$

where the mean and standard deviation (*SD*) are in terms of the measured fluorescence fold change ($\Delta F/F_0$). For the concentration series of S RBD analyte tested (**Figure 2d-e**), the *LOD* is calculated to be $\Delta F/F_0$ = 0.3456. This corresponds to an S RBD concentration of 12.59 nM based on the cooperative binding model fit.

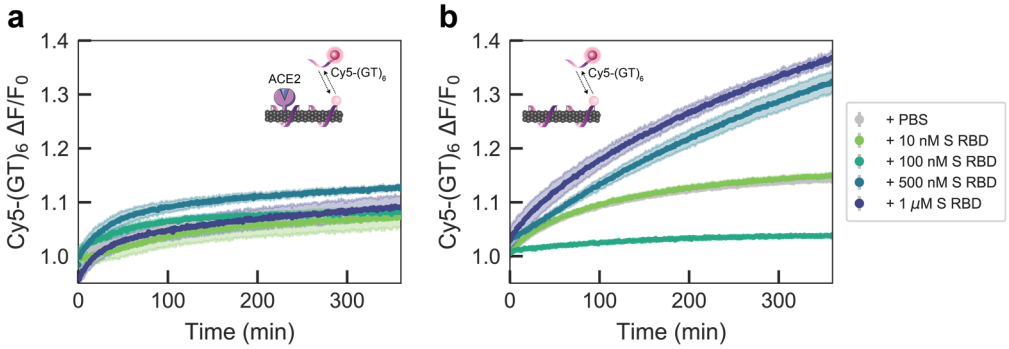

Figure S8. Displacement of Cy5-$(GT)_6$ ssDNA from SWCNT in the presence or absence of ACE2 sensing protein, as a function of S RBD analyte concentration. Addition of varying concentrations of S RBD analyte to **(a)** ACE2-Cy5-$(GT)_6$-SWCNT nanosensors (formed by 6.25 mg/L ACE2 and 2.5 mg/L $(GT)_6$-SWCNTs) and **(b)** Cy5-$(GT)_6$-SWCNTs alone (2.5 mg/L). Shaded error bars represent the standard error between experimental replicates (N = 3).

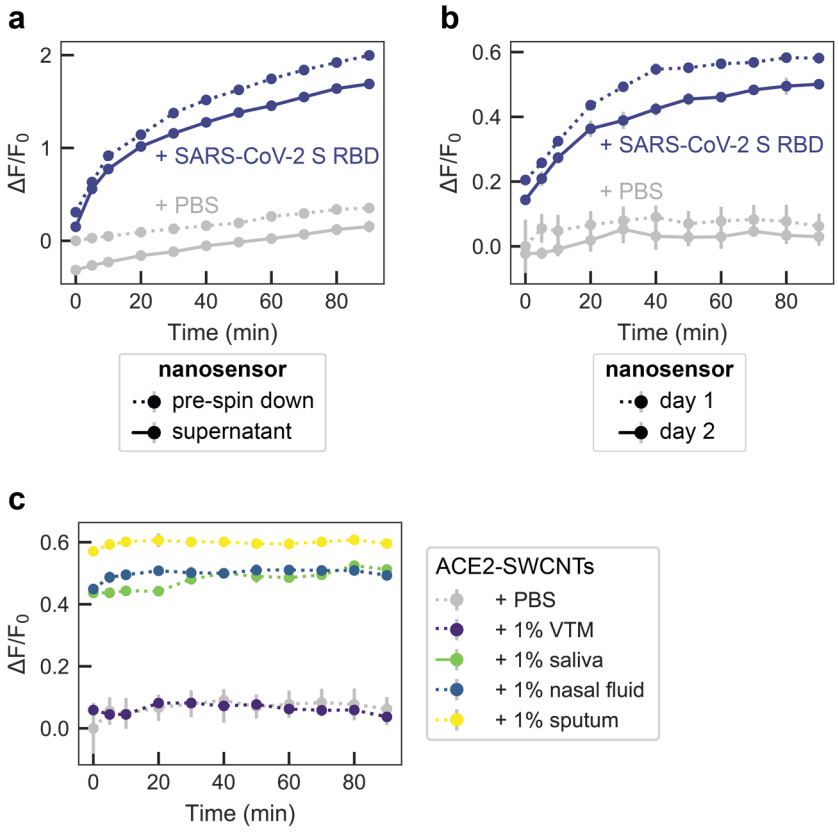

Figure S9. ACE2-SWCNT nanosensor controls for assessing stability. Response of ACE2-SWCNTs (formed by 6.25 mg/L ACE2 and 2.5 mg/L $(GT)_6$-SWCNTs) to S RBD was preserved **(a)** before and after centrifugation (16.1 krcf, 30 min; 500 nM S RBD) and **(b)** before and after overnight incubation at ambient conditions (1 μM S RBD). **(c)** Stability of ACE2-SWCNT nanosensors in different biofluids. Normalized change in fluorescence of the 1130 nm SWCNT emission peak for the ACE2-SWCNT sensor as a function of time in 1% relevant biofluids: viral transport medium (VTM), saliva, nasal fluid, and sputum (treated with sputasol). Nanosensor fluorescence in biofluids demonstrated stability yet elevated magnitudes. Gray bars represent standard error between experimental replicates (N = 3).

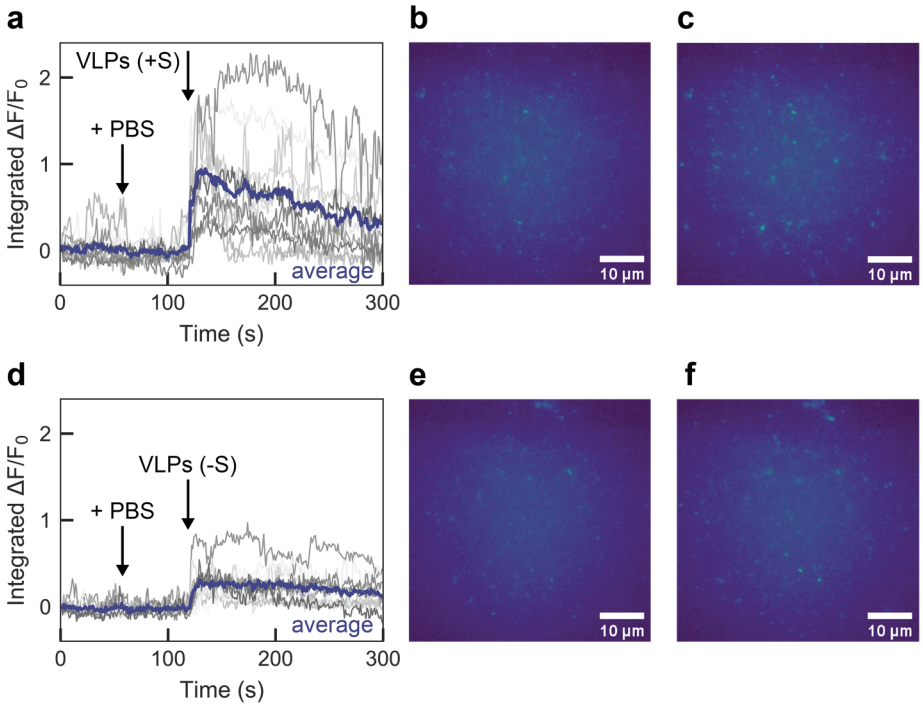

Figure S10. Surface-immobilized ACE2-SWCNT nanosensor response to SARS-CoV-2 virus-like particles (VLPs) with and without S protein. Microscopy traces of ACE2-SWCNTs (formed by 12.5 mg/L ACE2 and 5 mg/L $(GT)_6$-SWCNTs) immobilized on a glass-bottom microwell dish exhibited a larger fluorescence response to VLPs expressing S protein, for single regions of interest (gray; 12 total per image) and the average intensity (purple). **(a-c)** Addition of PBS at 60 s caused no change in fluorescence, as expected, and addition of 50 mg/L VLPs (with S protein) at 120 s yielded a large turn-on fluorescence response, as shown by **(a)** the integrated-fluorescence fold change ($\Delta F/F_0$) over 5 min and entire field-of-view at **(b)** time = 100 s and **(c)** time = 125 s. **(d-f)** Addition of PBS at 60 s caused no change in fluorescence, as expected, and addition of 50 mg/L VLPs (no S protein) at 120 s yielded a minor turn-on fluorescence response, as shown by **(d)** the integrated-fluorescence fold change ($\Delta F/F_0$) over 5 min and entire field-of-view at **(e)** time = 100 s and **(f)** time = 125 s. All fluorescence images were obtained with 721 nm laser excitation and a 100x oil immersion objective.

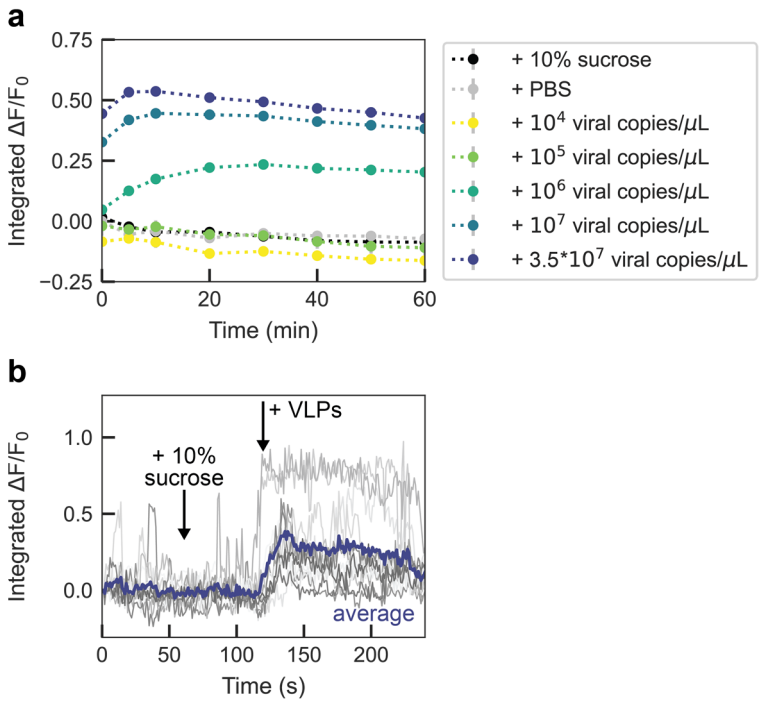

Figure S11. ACE2-SWCNT nanosensor response to lower concentrations of SARS-CoV-2 virus-like particles (VLPs). (a) Varying SARS-CoV-2 VLP concentrations were injected into ACE2-SWCNTs (formed by 6.25 mg/L ACE2 and 2.5 mg/L $(GT)_6$-SWCNTs) and the integrated-fluorescence fold change ($\Delta F/F_0$) was monitored over 60 min. Gray bars represent standard error between experimental replicates (N = 3). **(b)** Microscopy traces of ACE2-SWCNTs (formed by 12.5 mg/L ACE2 and 5 mg/L $(GT)_6$-SWCNTs) immobilized on a glass-bottom microwell dish exhibited a fluorescence response to 0.035 mg/L VLPs, for single regions of interest (gray; 12 total per image) and the average intensity (purple). Addition of 10% sucrose buffer (to match VLP buffer) at 60 s caused no change in fluorescence and addition of 0.035 mg/L VLPs (final concentration) at 120 s yielded a turn-on fluorescence response, as shown by the integrated-fluorescence fold change ($\Delta F/F_0$) over 4 min. Fluorescence spectra and images were obtained with 721 nm laser excitation, with **(a)** 10X and **(b)** 100X oil immersion objectives.

This platform for nanosensor design was expanded to attempt passivation of $(GT)_6$-SWCNTs with an antibody for SARS-CoV-1 S RBD that has been previously verified to bind CoV-2 S RBD.[12] Interestingly, the anti-S sensing protein did not exhibit any modulation in intrinsic SWCNT fluorescence, nor did addition of the S RBD analyte provoke a fluorescence response. This result, implying a lack of interaction between anti-S and the SWCNT surface, is in line with our previous work that implies antibodies exhibit minimal adsorption to ssDNA-SWCNTs.[13] Thus, alternative attachment strategies must be pursued for sensing proteins with no intrinsic affinity for the SWCNT surface.

Table S1. Purchased biofluid and protein specifications.

Purpose	Protein	Manufacturer	Lot #	Source	Form	Concentration
Sensing protein	Angiotensin-converting enzyme 2 (ACE2)	Ray Biotech	04U24020GC	Recombinant, (HEK293 cell expression system; C-terminal His-tag)	Liquid (PBS)	2.8 g/L
Control	SARS CoV-1 spike protein receptor-binding domain (CoV-1 S RBD)	ACROBiosystems	3558c-203KF1-R7	Recombinant (HEK293 cell expression system; C-terminal His-tag)	Lyophilized from PBS, 10% Trehalose	Reconstituted in 167 µL PBS, 30 min at room temperature with occasional gentle mixing
Control	MERS spike protein receptor-binding domain (MERS S RBD)	MyBioSource	0110YB	Recombinant (HEK293 cell expression system; C-terminal His-tag)	Liquid (PBS, 0.1% sodium azide)	1 g/L
Control	Influenza hemagglutinin subunit (FLU HA1)	MyBioSource	95-101-1104	Recombinant (E. coli expression; N-terminal His-tag and strepll-tag)	Liquid (PBS, 0.1% SDS, 0.02% sodium azide)	1 g/L
Control	Human serum albumin (HSA)	Sigma-Aldrich	#SLBZ2785	Human plasma	Lyophilized, fatty acid and globulin free	Reconstituted in PBS, 30 min at room temperature with occasional gentle mixing
Biofluid	Viral transport medium	Innovative Research	31975	Standard CDC-recommended formulation: 2% FBS, 100 µg/mL Gentamicin, 0.5 µg/mL Amphotericin in a Hanks Balanced salt solution base	Liquid	N/A
Biofluid	Saliva	Lee Biosolutions	W205820	Human, pooled, normal	Liquid	N/A
Biofluid	Nasal fluid	Lee Biosolutions	18-05-538	Human, single donor, normal	Liquid	N/A
Biofluid	Sputum	Lee Biosolutions	18-03-594	Human, single donor, normal	Liquid	N/A

Table S2. Comparison of sensor performance to current SARS-CoV-2 diagnostic technologies.

Type of test	Test name	Minimum detectable RNA (copies/µL)	Time per run (min)	Reference
Molecular				
RT-PCR	CDC PCR test	1	<180	[14,15]
	GenMark ePlex test	1	90	[16]
	Cepheid Xpert Xpress test	<1	45	[16]
Isothermal amplification	Abbott ID NOW test	20	15	[16]
	iLACO	10	20–40	[17]
(+CRISPR-based detection)	Mammoth Biosciences DETECTR	10	45	[18]
(+CRISPR-based detection)	Sherlock Biosciences CRISPR-based test	10	60	[19]
Next-generation sequencing	Nanopore Targeted Sequencing	<1	360-600	[20]
Antigen	Sofia 2, Quidel	595 (viral particles)	15	[14]
	FET biosensor	<1 (viral particles) / ~10^{-17} M - 10^{-15} (S)	<1	[21]
	OECT biosensor	~10^{-14} M (S RBD)	10	[22]
	SWCNT-based nanosensor	~10^{4} - 10^{6} (viral particles) / ~10^{-8} M (S RBD)	<1 (surface-immobilized) / 90 (well-plate)	this study

Note that prior work has established viral RNA load in SARS-CoV-2 infected human samples typically ranging from 10^{1}-10^{4} viral copies per µL.[23–26] These viral loads translate to approximately 10^{-15}-10^{-12} M S RBD.

References

(1) Jeng, E. S.-H. The Investigation of Interactions between Single Walled Carbon Nanotubes and Flexible Chain Molecules. Thesis, Massachusetts Institute of Technology, 2010.

(2) Amanat, F.; Stadlbauer, D.; Strohmeier, S.; Nguyen, T. H. O.; Chromikova, V.; McMahon, M.; Jiang, K.; Arunkumar, G. A.; Jurczyszak, D.; Polanco, J.; Bermudez-Gonzalez, M.; Kleiner, G.; Aydillo, T.; Miorin, L.; Fierer, D. S.; Lugo, L. A.; Kojic, E. M.; Stoever, J.; Liu, S. T. H.; Cunningham-Rundles, C.; Felgner, P. L.; Moran, T.; García-Sastre, A.; Caplivski, D.; Cheng, A. C.; Kedzierska, K.; Vapalahti, O.; Hepojoki, J. M.; Simon, V.; Krammer, F. A Serological Assay to Detect SARS-CoV-2 Seroconversion in Humans. *Nature Medicine* **2020**, *26* (7), 1033–1036. https://doi.org/10.1038/s41591-020-0913-5.

(3) Robbiani, D. F.; Gaebler, C.; Muecksch, F.; Lorenzi, J. C. C.; Wang, Z.; Cho, A.; Agudelo, M.; Barnes, C. O.; Gazumyan, A.; Finkin, S.; Hägglöf, T.; Oliveira, T. Y.; Viant, C.; Hurley, A.; Hoffmann, H.-H.; Millard, K. G.; Kost, R. G.; Cipolla, M.; Gordon, K.; Bianchini, F.; Chen, S. T.; Ramos, V.; Patel, R.; Dizon, J.; Shimeliovich, I.; Mendoza, P.; Hartweger, H.; Nogueira, L.; Pack, M.; Horowitz, J.; Schmidt, F.; Weisblum, Y.; Michailidis, E.; Ashbrook, A. W.; Waltari, E.; Pak, J. E.; Huey-Tubman, K. E.; Koranda, N.; Hoffman, P. R.; West, A. P.; Rice, C. M.; Hatziioannou, T.; Bjorkman, P. J.; Bieniasz, P. D.; Caskey, M.; Nussenzweig, M. C. Convergent Antibody Responses to SARS-CoV-2 in Convalescent Individuals. *Nature* **2020**, *584* (7821), 437–442. https://doi.org/10.1038/s41586-020-2456-9.

(4) Walls, A. C.; Park, Y.-J.; Tortorici, M. A.; Wall, A.; McGuire, A. T.; Veesler, D. Structure, Function, and Antigenicity of the SARS-CoV-2 Spike Glycoprotein. *Cell* **2020**, *181* (2), 281-292.e6. https://doi.org/10.1016/j.cell.2020.02.058.

(5) Wrapp, D.; Wang, N.; Corbett, K. S.; Goldsmith, J. A.; Hsieh, C.-L.; Abiona, O.; Graham, B. S.; McLellan, J. S. Cryo-EM Structure of the 2019-NCoV Spike in the Prefusion Conformation. *Science* **2020**, *367* (6483), 1260–1263. https://doi.org/10.1126/science.abb2507.

(6) Pinals, R. L.; Yang, D.; Lui, A.; Cao, W.; Landry, M. P. Corona Exchange Dynamics on Carbon Nanotubes by Multiplexed Fluorescence Monitoring. *J. Am. Chem. Soc.* **2020**, *142* (3), 1254–1264. https://doi.org/10.1021/jacs.9b09617.

(7) Yan, R.; Zhang, Y.; Li, Y.; Xia, L.; Guo, Y.; Zhou, Q. Structural Basis for the Recognition of SARS-CoV-2 by Full-Length Human ACE2. *Science* **2020**, *367* (6485), 1444–1448. https://doi.org/10.1126/science.abb2762.

(8) Pinals, R. L.; Chio, L.; Ledesma, F.; Landry, M. P. Engineering at the Nano-Bio Interface: Harnessing the Protein Corona towards Nanoparticle Design and Function. *Analyst* **2020**, *145* (15), 5090–5112. https://doi.org/10.1039/D0AN00633E.

(9) Alizadehmojarad, A. A.; Zhou, X.; Beyene, A. G.; Chacon, K. E.; Sung, Y.; Pinals, R. L.; Landry, M. P.; Vuković, L. Binding Affinity and Conformational Preferences Influence Kinetic Stability of Short Oligonucleotides on Carbon Nanotubes. *Advanced Materials Interfaces* **2020**, *7* (15), 2000353. https://doi.org/10.1002/admi.202000353.

(10) Beyene, A. G.; Alizadehmojarad, A. A.; Dorlhiac, G.; Goh, N.; Streets, A. M.; Král, P.; Vuković, L.; Landry, M. P. Ultralarge Modulation of Fluorescence by Neuromodulators in Carbon Nanotubes Functionalized with Self-Assembled Oligonucleotide Rings. *Nano Lett.* **2018**, *18* (11), 6995–7003. https://doi.org/10.1021/acs.nanolett.8b02937.

(11) Long, G. L.; Winefordner, J. D. Limit of Detection A Closer Look at the IUPAC Definition. *Analytical chemistry* **1983**, *55* (7), 712A-724A.

(12) Yuan, M.; Wu, N. C.; Zhu, X.; Lee, C.-C. D.; So, R. T. Y.; Lv, H.; Mok, C. K. P.; Wilson, I. A. A Highly Conserved Cryptic Epitope in the Receptor Binding Domains of SARS-CoV-2 and SARS-CoV. *Science* **2020**, *368* (6491), 630–633. https://doi.org/10.1126/science.abb7269.

(13) Pinals, R. L.; Yang, D.; Rosenberg, D. J.; Chaudhary, T.; Crothers, A. R.; Iavarone, A. T.; Hammel, M.; Landry, M. P. Quantitative Protein Corona Composition and Dynamics on Carbon Nanotubes in Biological Environments. *Angewandte Chemie International Edition* **2020**, *59* (52), 23668–23677. https://doi.org/10.1002/anie.202008175.

(14) Guglielmi, G. The Explosion of New Coronavirus Tests That Could Help to End the Pandemic. *Nature* **2020**, *583* (7817), 506–509. https://doi.org/10.1038/d41586-020-02140-8.

(15) CDC 2019-Novel Coronavirus (2019-NCoV) Real-Time RT-PCR Diagnostic Panel.

(16) Zhen, W.; Smith, E.; Manji, R.; Schron, D.; Berry, G. J. Clinical Evaluation of Three Sample-to-Answer Platforms for Detection of SARS-CoV-2. *Journal of Clinical Microbiology* **2020**, *58* (8). https://doi.org/10.1128/JCM.00783-20.

(17) Yu, L.; Wu, S.; Hao, X.; Dong, X.; Mao, L.; Pelechano, V.; Chen, W.-H.; Yin, X. Rapid Detection of COVID-19 Coronavirus Using a Reverse Transcriptional Loop-Mediated Isothermal Amplification (RT-LAMP) Diagnostic Platform. *Clin Chem* **2020**, *66* (7), 975–977. https://doi.org/10.1093/clinchem/hvaa102.
(18) Broughton, J. P.; Deng, X.; Yu, G.; Fasching, C. L.; Servellita, V.; Singh, J.; Miao, X.; Streithorst, J. A.; Granados, A.; Sotomayor-Gonzalez, A.; Zorn, K.; Gopez, A.; Hsu, E.; Gu, W.; Miller, S.; Pan, C.-Y.; Guevara, H.; Wadford, D. A.; Chen, J. S.; Chiu, C. Y. CRISPR–Cas12-Based Detection of SARS-CoV-2. *Nature Biotechnology* **2020**, *38* (7), 870–874. https://doi.org/10.1038/s41587-020-0513-4.
(19) Zhang, F.; Abudayyeh, O. O.; Gootenberg, J. S. A Protocol for Detection of COVID-19 Using CRISPR Diagnostics. 8.
(20) Wang, M.; Fu, A.; Hu, B.; Tong, Y.; Liu, R.; Liu, Z.; Gu, J.; Xiang, B.; Liu, J.; Jiang, W.; Shen, G.; Zhao, W.; Men, D.; Deng, Z.; Yu, L.; Wei, W.; Li, Y.; Liu, T. Nanopore Targeted Sequencing for the Accurate and Comprehensive Detection of SARS-CoV-2 and Other Respiratory Viruses. *Small* **2020**, *16* (32), 2002169. https://doi.org/10.1002/smll.202002169.
(21) Seo, G.; Lee, G.; Kim, M. J.; Baek, S.-H.; Choi, M.; Ku, K. B.; Lee, C.-S.; Jun, S.; Park, D.; Kim, H. G.; Kim, S.-J.; Lee, J.-O.; Kim, B. T.; Park, E. C.; Kim, S. I. Rapid Detection of COVID-19 Causative Virus (SARS-CoV-2) in Human Nasopharyngeal Swab Specimens Using Field-Effect Transistor-Based Biosensor. *ACS Nano* **2020**, *14* (4), 5135–5142. https://doi.org/10.1021/acsnano.0c02823.
(22) Guo, K.; Wustoni, S.; Koklu, A.; Díaz-Galicia, E.; Moser, M.; Hama, A.; Alqahtani, A. A.; Ahmad, A. N.; Alhamlan, F. S.; McCulloch, I.; Arold, S. T.; Grünberg, R.; Inal, S. A Nanobody-Functionalized Organic Electrochemical Transistor for the Rapid Detection of SARS-CoV-2 or MERS Antigens at the Physical Limit. *medRxiv* **2020**, 2020.11.12.20228874. https://doi.org/10.1101/2020.11.12.20228874.
(23) Zou, L.; Ruan, F.; Huang, M.; Liang, L.; Huang, H.; Hong, Z.; Yu, J.; Kang, M.; Song, Y.; Xia, J.; Guo, Q.; Song, T.; He, J.; Yen, H.-L.; Peiris, M.; Wu, J. SARS-CoV-2 Viral Load in Upper Respiratory Specimens of Infected Patients. *New England Journal of Medicine* **2020**, *382* (12), 1177–1179. https://doi.org/10.1056/NEJMc2001737.
(24) Pan, Y.; Zhang, D.; Yang, P.; Poon, L. L. M.; Wang, Q. Viral Load of SARS-CoV-2 in Clinical Samples. *The Lancet Infectious Diseases* **2020**, *20* (4), 411–412. https://doi.org/10.1016/S1473-3099(20)30113-4.
(25) To, K. K.-W.; Tsang, O. T.-Y.; Leung, W.-S.; Tam, A. R.; Wu, T.-C.; Lung, D. C.; Yip, C. C.-Y.; Cai, J.-P.; Chan, J. M.-C.; Chik, T. S.-H.; Lau, D. P.-L.; Choi, C. Y.-C.; Chen, L.-L.; Chan, W.-M.; Chan, K.-H.; Ip, J. D.; Ng, A. C.-K.; Poon, R. W.-S.; Luo, C.-T.; Cheng, V. C.-C.; Chan, J. F.-W.; Hung, I. F.-N.; Chen, Z.; Chen, H.; Yuen, K.-Y. Temporal Profiles of Viral Load in Posterior Oropharyngeal Saliva Samples and Serum Antibody Responses during Infection by SARS-CoV-2: An Observational Cohort Study. *The Lancet Infectious Diseases* **2020**, *20* (5), 565–574. https://doi.org/10.1016/S1473-3099(20)30196-1.
(26) Wyllie, A. L.; Fournier, J.; Casanovas-Massana, A.; Campbell, M.; Tokuyama, M.; Vijayakumar, P.; Warren, J. L.; Geng, B.; Muenker, M. C.; Moore, A. J.; Vogels, C. B. F.; Petrone, M. E.; Ott, I. M.; Lu, P.; Venkataraman, A.; Lu-Culligan, A.; Klein, J.; Earnest, R.; Simonov, M.; Datta, R.; Handoko, R.; Naushad, N.; Sewanan, L. R.; Valdez, J.; White, E. B.; Lapidus, S.; Kalinich, C. C.; Jiang, X.; Kim, D. J.; Kudo, E.; Linehan, M.; Mao, T.; Moriyama, M.; Oh, J. E.; Park, A.; Silva, J.; Song, E.; Takahashi, T.; Taura, M.; Weizman, O.-E.; Wong, P.; Yang, Y.; Bermejo, S.; Odio, C. D.; Omer, S. B.; Dela Cruz, C. S.; Farhadian, S.; Martinello, R. A.; Iwasaki, A.; Grubaugh, N. D.; Ko, A. I. Saliva or Nasopharyngeal Swab Specimens for Detection of SARS-CoV-2. *New England Journal of Medicine* **2020**, *383* (13), 1283–1286. https://doi.org/10.1056/NEJMc2016359.